Moisture and ion transport properties in blended pastes and their relation to the refined pore structure

(article starts on next page)

Moisture and ion transport properties in blended pastes and their relation to the refined pore structure

Liming Huang [a,b,*], Luping Tang [a], Ingemar Löfgren [a,c], Nilla Olsson [d], Zhenghong Yang [b], Yongqiang Li [e]

[a] *Department of Architecture and Civil Engineering, Chalmers University of Technology, 41296 Gothenburg, Sweden*
[b] *Key Laboratory of Advanced Civil Engineering Materials Ministry of Education, Tongji University, Shanghai 201804, PR China*
[c] *Thomas Concrete Group AB, Södra Vägen 28, 41707 Gothenburg, Sweden*
[d] *Division Building Sweden, NCC Building, 17080 Solna, Sweden*
[e] *College of Civil and Transportation Engineering, Shenzhen University, Shenzhen 518060, Guangdong, PR China*

ARTICLE INFO

ABSTRACT

This paper presents a study of the moisture transport properties in blended pastes measured by a new procedure and setup. The dependence of moisture transport coefficient on relative humidity (RH) is confirmed. The differences in the moisture dependency may be due to discrepancies in the critical RH for the percolation of liquid. Fly ash and slag increase the percentage of mesopores or "ink-bottle" pores with a mesoscale neck and they strongly reduce the pore connectivity in pastes. These effects cause the evident reduction in the moisture and chloride diffusivity. The additional replacement with limestone filler has little effect on the pore connectivity. The formation factor controls the moisture transport at the high RH interval, but the volume of small pores (middle capillary and mesopores) is the major determinant at a low RH interval. The relationship between water-binder ratio, pore structure and moisture transport or chloride migration coefficient is discussed.

1. Introduction

Moisture content and transport properties in cement-based materials are essential parameters during the construction and long-term use of concrete structures. The humidity conditions in concrete substrate before applying a covering material is directly related to the risk of moisture damage and mould growth [1]. Moreover, these properties of cement-based materials make an impact on the transport of CO_2, O_2 and chloride ions in concrete, which determines the deterioration process of reinforced concrete structures [2,3]. Reliable moisture transport parameters are critical for not only ensuring the appropriate construction schedule but also the accurate prediction of the service life of concrete structures.

The transport of condensable vapors through a microporous substance is a complex process that involves vapor diffusion, surface diffusion, condensation, evaporation, and flow of liquid and depends on the RH in materials [4]. The condensation and evaporation rates may be negligible compared to the diffusion process [5], but the volume of pores with the condensed liquid determines the connectivity of empty pores that influences the diffusion process. The condensed volume of water

(namely, the moisture content) relates not only to the microstructure in cement-based material but also to the ion concentration in pore solution [6]. The blending of supplementary cementitious materials (SCMs) is efficient in reducing CO_2 emissions in the cement industry [7], so an increasing amount of fly ash, slag, limestone, and calcined clay has been blended into cement to produce more sustainable concrete. SCMs modify the microstructure [8–10] and the pore solution in cement-based materials [11], leading to different moisture and ion transport properties compared to the ordinary Portland cement (OPC) concrete. The lack of knowledge about the moisture fixation and transport performance in sustainable concrete has caused some clients and contractors to worry about the application of the blended cement in constructions [12].

Many papers investigated the reduction effect of SCMs on the chloride migration in cement-based materials from the experimental investigation or modeling aspect [13–18]. However, there were a limited number of papers that studied the effect of SCMs on the moisture transport performance. Baroghel-Bouny [2] found that the apparent moisture diffusion coefficient of concrete with 8 %-10 % silica fume is lower than the reference concrete when the water saturation degree is larger than 50 %. Saeidpour and Wadsö [19] used a modified cup

---

method to investigate the difference between the vapor diffusion coefficient of the blended mortar in adsorption and desorption processes. Their results indicated that both silica fume and slag induced a one order of magnitude reduction in the vapor transport coefficient in both adsorption and desorption processes. They ascribed this effect to the higher amount of gel pores and lower volume of capillary pores in the blended system. The same reduction effects from silica fume and slag were also reported in the investigation by Olsson et al. [20], and this effect is more evident at higher RH levels. The authors tried to correlate the difference in the moisture diffusion rate with the difference in the structure of C-S-H in the hydration products, but no plausible correlation was concluded. The high moisture resistance in the blended system may mainly come from its refinement of the pore structure. This was also mentioned in the discussion part of other published papers [19–21], but which parameter relating to the pore structure should be used to correlate with vapor diffusion has not been clearly established. There are many parameters to describe the pore structure in cement-based materials: porosity, pore size distribution, pore connectivity, tortuosity, the critical entry pore size (CP) and formation factor (*FF*). The decrease of CP was raised as the reason for forcing the vapor transport through the smaller pores in the blended mortar than in OPC [20,21] because Berodier and Scrivener [9] found that slag reduced the CP of pastes cured in water for 28 days. However, paste with fly ash normally has a similar and even larger CP compared to OPC paste before 90 days [9,22]. It indicates that the decrease in CP can hardly explain the much lower vapor diffusion in the fly ash blended mortar than OPC.

Some numerical simulations were performed to predict the vapor diffusion or relative permeabilities of OPC concrete based on the pore size distribution [23] or pore network [24]. However, these models may not fit for the blended system because of the minor differences in the pore size distribution and the huge differences in moisture transport properties especially at high RH compared to OPC. Therefore, it is of great significance to find some comprehensive parameters that can effectively indicate the vapor transport performance. The *FF* is one of the comprehensive parameters, and it is closely related to the mass transport inside the porous materials. As Eq. (1) shows, it is correlated to both porosity (Φ) and pore connectivity (β) [25,26], which also has a relation with ionic conductivity and the ion transport properties as highlighted in [27].

$$FF = \frac{\sigma_{ps}}{\sigma_p} = \frac{D_{ps}}{D_p} = \frac{1}{\Phi\beta} \tag{1}$$

where σ_{ps} is the electrical conductivity of pore solution and σ_p is the electrical conductivity of paste. D_{ps} and D_p are the diffusivity of the ions in the bulk pore solution and paste, respectively.

This paper aims to reveal the relationship between the moisture or chloride ion transport properties measured in laboratory and the pore structure parameters in both the OPC and blended pastes, so that the engineers and scientists can better predict the drying process and service life of the concrete. There are several methods to determine the moisture transport properties in porous materials based on steady-state conditions (constant flux through the samples, such as the cup method [28]) or non-steady-state conditions (such as semi-infinite drying [2]). The cup method takes a long time (>5 months) to get the equilibrium for a constant flux, which also strongly depends on the sample dimensions. The semi-infinite drying method may be much faster than the cup method, but it relies heavily on the initial humidity control of the sample [29]. In certain RH intervals, the vapor diffusion coefficient (D_v) from the cup method may be comparable with the value calculated by using the moisture content and the moisture transport coefficient (D_w) from the semi-infinite drying method [30,31]. Saeidpour and Wadsö [32] used small samples of cement paste and found that an unsteady-state method could not give a result that was evaluated by methods based on Fick's law due to the anomalous diffusion. This also indicates that results from the steady-state and unsteady-state method will be difficult

to compare (at least for small samples).

A new procedure and setup for the moisture diffusion test of pastes are described in this paper. It enables to measure both D_v and D_w of the same sample in one procedure. The chloride migration coefficient was measured by the rapid chloride migration method (RCM) [33]. The pore size distribution in hardened pastes was measured by the mercury intrusion porosimeter (MIP). The refinement effect of SCMs on the pore structure in pastes is discussed by the interpretation of different parameters. The differences in moisture and chloride transport in pastes blended with different SCMs are comprehensively compared to the pore structure parameters in the final part of the discussion.

2. Materials and methods

2.1. Materials

OPC is CEM I 52.5 R with a Blaine surface of 525 m^2/kg. OPC was mixed with three different SCMs (slag, fly ash and limestone). Slag (SL) with a Blaine surface of 420 m^2/kg was obtained from Thomas Cement AB company. Fly ash (FA) was from Cementa, and limestone with $D_{50} = 18$ μm (LL) was supplied by Nordkalk.

Table 1 shows the chemical composition of all binders. Table 2 presents the mix proportions of the 11 samples. In the binary systems, OPC was replaced with 35 % FA (P1) or SL (P2). OPC was replaced with 35 % slag and 16 % limestone to obtain a ternary system (P3). Pastes were mixed with three different water-binder ratios (*w/b*) of 0.35, 0.45 and 0.55, respectively, except for P1 with only two *w/b* (0.35 and 0.45).

2.2. Methods

2.2.1. Preparation of pastes

The pastes were homogeneously mixed in the planetary mixer whose stirring rate can be continuously adjusted. For a good homogeneity of mixing, 100 stainless steel balls (16 mm diameter) were added in the bowl. The speed of the agitator was controlled with about 75 rpm and 7 rotations per revolution to avoid bouncing of the balls. OPC paste (P0) with *w/b* = 0.35 was mixed for 1 min after the addition of all the deionized water in the bowl with OPC. A rubber scrapper was used to move the materials adhering on the wall and in the bottom to the middle. Afterwards the paste was mixed for another 2 min. The pastes with *w/b* = 0.45 were firstly mixed with the amount of water equal to *w/b* = 0.35 for 1 min. Afterwards, the slurry was scraped with the rubber scrapper as described above. Then, the remaining amount of water was added and mixed for another 1 min. After a second scraping, the paste was mixed for another 2 min. The pastes with *w/b* = 0.55 were firstly mixed with the amount of water equal to *w/b* = 0.35 for 1 min. After the first scraping, the water was added up to *w/b* = 0.45 followed a 1 min mixing and a second scraping. Finally, the rest of the water was added and mixed for 1 min. After the third scraping, the paste was mixed for another 2 min. The paste was taken out to cast in the polypropylene tubes shown in Fig. 1. For the blended pastes, an extra 1 min premix of

Table 1
Chemical composition of different binders (*LOI*: loss of ignition).

Chemical Composition (wt%)	CEM I 52.5 R	Slag	Fly ash	Limestone
CaO	62.20	39.11	5.10	49.50
SiO$_2$	19.60	36.63	54.62	9.00
Al$_2$O$_3$	4.50	13.56	22.41	0.60
Fe$_2$O$_3$	3.00	0.49	8.68	0.30
SO$_3$	3.50	0.27	0.80	0.03
MgO	3.50	8.52	1.79	–
K$_2$O	1.01	0.57	2.10	0.30
Na$_2$O	0.27	0.42	1.00	0.10
Cl	0.07	0.01	–	–
Sulfide	–	0.73	–	
LOI	2.50	−1.07	3.50	40.17

Table 2
The mix proportion of the 11 different samples.

Samples	*w/b*	Binders (by weight)			
		CEM I 52.5 R	Fly ash	Slag	Limestone
P035	0.35				
P045	0.45	100 %	–	–	–
P055	0.55				
P135	0.35				
P145	0.45	65 %	35 %	–	–
P235	0.35				
P245	0.45	65 %	–	35 %	–
P255	0.55				
P335	0.35				
P345	0.45	49 %	–	35 %	16 %
P355	0.55				

the dry binder was performed before adding the water. Afterwards, the blended pastes were mixed by following the same protocol as the OPC pastes. To avoid inhomogeneity caused by bleeding, the sealed tubes with fresh paste were put on the rotator with a speed of 12 rpm for 24 h. Finally, the samples were stored in the curing room with a constant temperature of 20 °C for 390 days.

2.2.2. Procedures and setup for the moisture diffusion test

After curing for 390 days, the tubes were wet cut from the top with a constant water flow using an electric diamond saw. Firstly, we cut a thin layer from the surface (~3 mm) to make an even surface. Afterwards, three discs with a thickness of about 7 mm were cut for the vapor diffusion measurement (shown in Fig. 1). The actual thickness (*h*) and diameter (*D*) of the discs were measured at 4 different places to take an average value. The rest of the sample was used to do the semi-infinite drying measurement. Both the discs and the rest of samples were conditioned under RH = 97.6 % for 14 days. Before the discs were mildly pressed in the tubes with the saturated salt solution for different RH control, a layer of watertight tape (double side, Stokvis VST397F1210) was adhered around the side of the disc. The head and tail of the tape were connected without any gap or overlapping (a "slash" shape in Fig. 1). Two dummy disc samples (engineering plastic, acetal

copolymer) were used to check the leakage of the sealing tapes at each RH intervals. The tape was adhered around the side of the dummy samples, and then the dummy sample was mounted in the tubes.

After the sample was mounted into the tubes, the distance between the solution surface and disc (*L*) was measured. The RH in the tubes and conditioning box was controlled by use of the saturated salt solutions: NaCl (75.5 %), KCl (85.1 %) and K_2SO_4 (97.6 %) at 20 °C [34]. Vapor diffusion in the pastes was measured under 4 different RH intervals, 97.6–75.5 % (RH97-75), 85.1–75.5 % (RH85-75), 97.6–50 % (RH97-50) and 75.5–50 % (RH75-50). The semi-infinite drying was conducted under two different RH conditions (75.5 % in the box and 50 % in the climate room). To avoid any leakage from the edge of the tubes, a thin circle of watertight adhesive (LOCTITE® 60 Seconds Universal glue) was applied around the edge. All the tubes were weighed at a sequence of conditioning times. We took 3 parallel measurements and some of the original data is presented in Fig. S1 and S2 (Supplementary information).

2.2.3. Moisture content test

Pastes were also crushed into particles (<2 mm) and then conditioned in the box with different RH controls (97.6 %, 75.5 % and 50 %, respectively). Calcium hydroxide was put in the climate box as a sacrifice to absorb CO_2. The RH in the conditioning box was monitored by the RH sensors (testo 174H). After 1 year conditioning, the particles were used to measure the evaporable water content by vacuum drying at 60 °C for 3 days.

2.2.4. Rapid chloride migration test

Pastes were mixed by following the same protocols described in Section 2.1, and then a rubber cylinder mould (*inner diameter of* 50 mm, *h*eight of 110 mm) was used to cast the samples. After the sealed curing for 1 day, samples were demoulded and put into a moist curing for 28 days and 90 days. At the specified age, two samples with a thickness of 50 mm were cut from each specimen for the RCM test. The test was performed according to NT BUILD 492 but without the vacuum saturation procedure because the specimens were moist cured before the test.
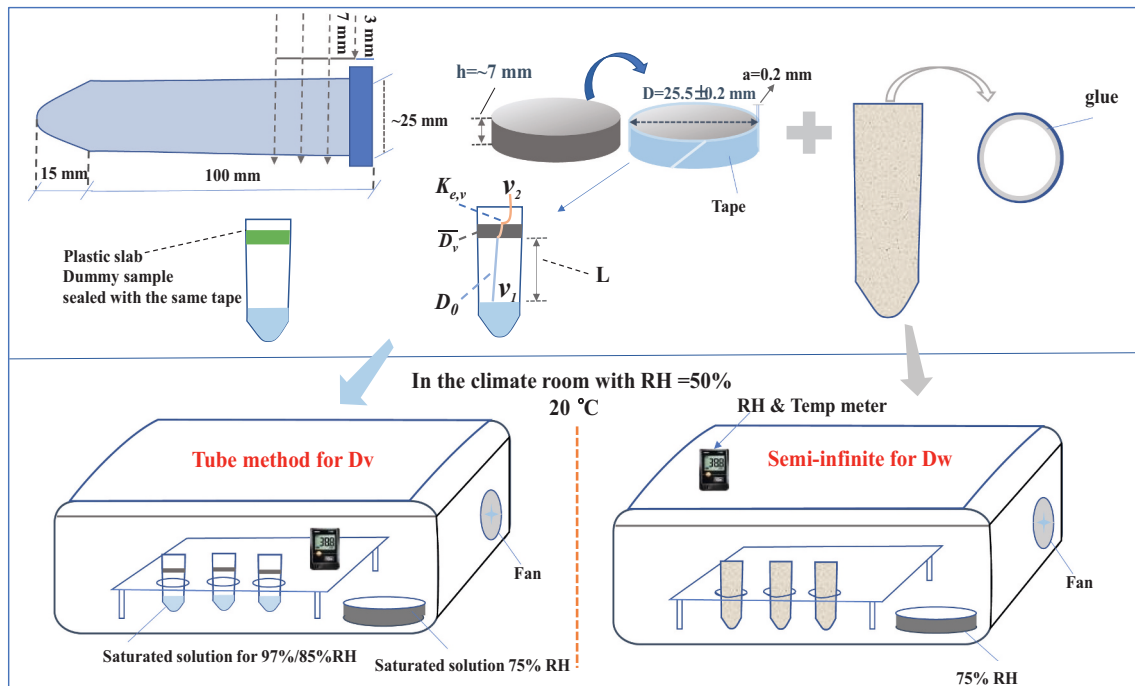
Fig. 1. A sketch of the new method for measuring the moisture diffusivity of pastes.

2.2.5. Electrical conductivity

The electrical conductivity of the pastes was tested by Wenner's four electrodes method which was detailly described in one previous paper [35]. The conductivity data at 28, 90, and 365 days were collected. The conductivity of the pore solution was calculated according to the empirical function in [35].

2.2.6. MIP measurement

After crushing, the pieces of 3–8 mm size were selected by sieving. Afterwards, the hydration of the samples was stopped by immersing the pieces into isopropanol for 3 days, which duration is appropriate for a full solvent exchange [36]. The pieces were then dried with continuous pumping under vacuum at 40 °C for 3 days. The pore size was measured by a MicroActive AutoPore V 9600 Version 2.03 machine. The pressure was initiated at 0.003 Pa and increased up to 250 MPa, which allows for the intrusion of pore entries from 373 μm initially down to about 6 nm (contact angle of 138°).

2.2.7. Calculation of the moisture transport properties

The related abbreviations are summarized in Table 3. During the semi-infinite drying process, the moisture content was considered as the driving force for moisture transport in this non-steady-state conditions. The one-dimensional diffusion can be described by Fick's second law as Eq. (2).

$$\frac{\partial C}{\partial t} = \frac{\partial^2 C}{\partial x^2} \tag{2}$$

The distribution of moisture content inside pastes is an analytical solution of the above equation with the boundary condition: $C = C_1$; $x = 0$; $t > 0$, and the initial condition: $C = C_0$; $x > 0$; $t = 0$. Hence, its distribution inside the paste follows Eq. (3) [30,37].

$$\frac{(C - C_1)}{(C_0 - C_1)} = erf \frac{x}{2\sqrt{D_w t}} \tag{3}$$

where C_0 and C_1 (kg/m^3) are the initial moisture content in the pastes (moisture content at RH = 97 % in this paper) and moisture content on the drying surface (moisture content at RH = 50 % or 75 %), respectively. The "x"is the distance from the surface to the inside position where the moisture content is C. D_w (m^2/s) is the moisture transport coefficient and t (s) is the duration of the drying time. The loss of

Table 3
Abbreviations of the terminology.

Abbreviation	Meaning of it
CP	The critical entry pore size
FF	Formation factor
Φ	Porosity
β	Pore connectivity
σ_{ps}	The electrical conductivity of pore solution
σ_p	The electrical conductivity of paste
D_{ps}	The diffusivity of ions in pore solution
D_p	The diffusivity of ions in paste
D_v	The vapor diffusion coefficient
$\overline{D_v}$	The average vapor diffusion coefficient
D_w	The moisture transport coefficient
C_0	The initial moisture content in pastes before drying
C_1	Moisture content on the drying surface
k_w	Drying coefficient
$D_{v,s}$	The vapor diffusion coefficient during semi-infinite drying
W_i	Water content in paste conditioned at relative humidity of φ_i
v_i	Moisture content in air at relative humidity of φ_i
$K_{e,v}$	The surface moisture resistance
$j_{v,\,t_i}$	Water vapor flux at the time interval t_{i-1} to t_i
D_0	The diffusion coefficient of water vapor in air
D_s	The moisture diffusion coefficient in the saturated paste
D_{v0}	The moisture diffusion coefficient in the dry paste (0 % RH)
φ_c	The critical relative humidity for percolation of liquid in paste
D_{RCM}	The chloride migration coefficient tested by RCM

diffusing substance from the semi-infinite medium is given by

$$\left(D_w \frac{\partial C}{\partial x}\right)_{x=0} = \frac{D_w(C_0 - C_1)}{\sqrt{\pi D_w t}} \tag{4}$$

An integral of Eq. (4) from zero time to t can get:

$$M_t = 2(C_0 - C_1)\sqrt{\frac{D_w t}{\pi}} = k_w \sqrt{t} \tag{5}$$

M_t (kg/m^2) is the moisture loss of the samples drying to time t. Furthermore, we can get the drying coefficient k_w by the regression of moisture loss (M_t) and $\sqrt{t}$ (see Fig. S3 in supplementary information). Thereafter, the total moisture transport coefficient D_w can be obtained by Eq. (6).

$$D_w = \frac{\pi k_w^2}{4(C_0 - C_1)^2} \tag{6}$$

The vapor diffusion coefficient $D_{v,s}$ (m^2/s) during semi-infinite drying was defined as [38]:

$$D_{v,s} = \frac{D_w}{v_s} * \frac{dW}{d\varphi} \tag{7}$$

where $dW/d\varphi$ is the moisture capacity of the pastes (data shown in Table S1 and S2 in supplementary information). Herein, the average moisture capacity was used as shown in Eq. (8). W_1 and W_2 are the moisture content in cement pastes conditioned under φ_1 and φ_2, respectively. It is calculated by Eq. (9).

$$\frac{dW}{d\varphi} = \frac{W_2 - W_1}{\varphi_2 - \varphi_1} \tag{8}$$

$$W_i = \frac{m_i - m_0}{\frac{m_0}{\rho_0}} = \frac{\rho_0(m_i - m_0)}{m_0} \tag{9}$$

where m_i is the weight of the pastes conditioned at RH = φ_i, m_0 is the weight of the pastes vacuum dried at 60 °C and ρ_0 is the bulk density of the vacuum dried pastes.

Generally, the vapor diffusion through the disc samples obeys Fick's first law

$$j_{v,t_i} = \overline{D_{v,t_i}} \frac{\Delta v}{h} \tag{10}$$

where $j_{v,\,t_i}$ is the vapor flux during the diffusion from time t_{i-1} to t_i. t_i corresponds to the latest time weighing the tubes, Δv (kg/m^3) is the difference in the vapor content between the upper and lower surfaces of the specimens and h (m) is the thickness of disc. The leakage of dummy sample, Δm_{dt} (kg), was included in the calculation of the vapor flux from t_{i-1} to $t_i.j_{v,\,t_i}$, so it can be calculated by Eq. (11).

$$j_{vt} = \frac{\Delta m_{st} - \Delta m_{dt}}{A\Delta t} \tag{11}$$

where $\overline{D_{v,t_i}}$ (m^2/s) is the average vapor diffusion coefficient between t_{i-1} and t_i and Δm_{st} (kg) is the weight loss of tubes with discs of pastes from t_{i-1} to t_i. The surface vapor content is not so easy to measure, but the vapor content on the surface of the saturated salt solution and in the climate box (room) can be calculated by

$$v_i = v_s * \varphi_i \tag{12}$$

where v_i is the moisture content in air at the corresponding RH and v_s is the saturation moisture content in air (17.28 g/m^3 at 20 °C). Therefore, considering the surface moisture resistance ($K_{e,v}$) and moisture transport in tube air, the mass flux from the saturated salt solution to the climate box reads

$$j_{v,t_i} = \frac{v_2 - v_1}{\frac{h}{D_{v,t_i}} + \frac{L}{D_0} + \frac{1}{K_{e,v}}} \tag{13}$$

The $K_{e,v}$ is approximately 0.007 m/s [19] for the discs with the similar size in this investigation. With the weight loss change (see Fig. S2 in supplementary information) substituting into Eq. (11), we can use Eqs. (12) and (13) to calculate the average vapor diffusion coefficient from the tube method.

3. Results

3.1. Semi-infinite drying diffusivity (D_w and $D_{v,s}$)

Fig. 2 shows the moisture diffusion coefficient (D_w) and vapor diffusion coefficient ($D_{v,s}$) determined by the semi-infinite drying method. All the pastes dried at 75 % RH have a lower D_w than those dried at 50 % RH. The D_w, which was also called the apparent moisture diffusion coefficient in [2,39], was found to be moisture dependent in cement-based materials. It decreased as the saturation degree increased from zero and reached the minimum value at some middle degree (0.5–0.8). After the percolation of liquid was reached at this critical value, D_w increased with the saturation degree. The specific value of this critical saturation degree might be related to the structure of the hydration products, such as the volume of high density (HD) C-S-H [2]. The blending of FA and SL in pastes increases the volume of HD C-S-H [40].

Their D_w has a larger difference at 50 % and 75 % RH compared to OPC pastes (see Fig. 2a), and this effect is similar to that of silica fume [2].

The pastes with a higher w/b show a higher D_w. The blending of SCMs presents a significant reduction in the D_w during both 50 % and 75 % RH drying. To obtain a normalized value, the transport coefficients of the blended pastes have been calculated by dividing them with these co-efficients of the OPC pastes with the same w/b. The normalized factor of D_w at 75 % RH is in the range of 0.05–0.18 (see Fig. 2c), and the factor shows a decreasing trend as w/b increases, except for the ternary paste. The ternary paste shows the lowest D_w among the pastes with $w/b = 0.35$. When w/b is 0.45 and 0.55, the SL binary pastes have the lowest value compared to the other pastes. The further replacement of OPC by LL increases the moisture transport coefficient. While drying at RH = 50 %, the blended pastes present a higher normalized factor compared to 75 % RH. The factors of FA or SL binary pastes stay in a range of 0.18–0.27, and the FA blended paste with $w/b = 0.45$ has the lowest factor. A further blending of LL increases the factor of D_w to a range of 0.38–0.54, which is almost twice the factor of the SL binary paste.

$D_{v,s}$ and its normalized factor are presented in Fig. 2b and d, respectively. The drying RH has the similar effect on $D_{v,s}$ as on D_w, but the discrepancy in $D_{v,s}$ at the different RH is smaller than that in D_w. This phenomenon is more evident in the blended paste mainly due to the higher moisture capacity ($dW/d\varphi$) in blended pastes compared to OPC (see Table S1 and S2 in supplementary information). Some published papers [20,41] also found that the blended pastes (SL/silica fume) had a
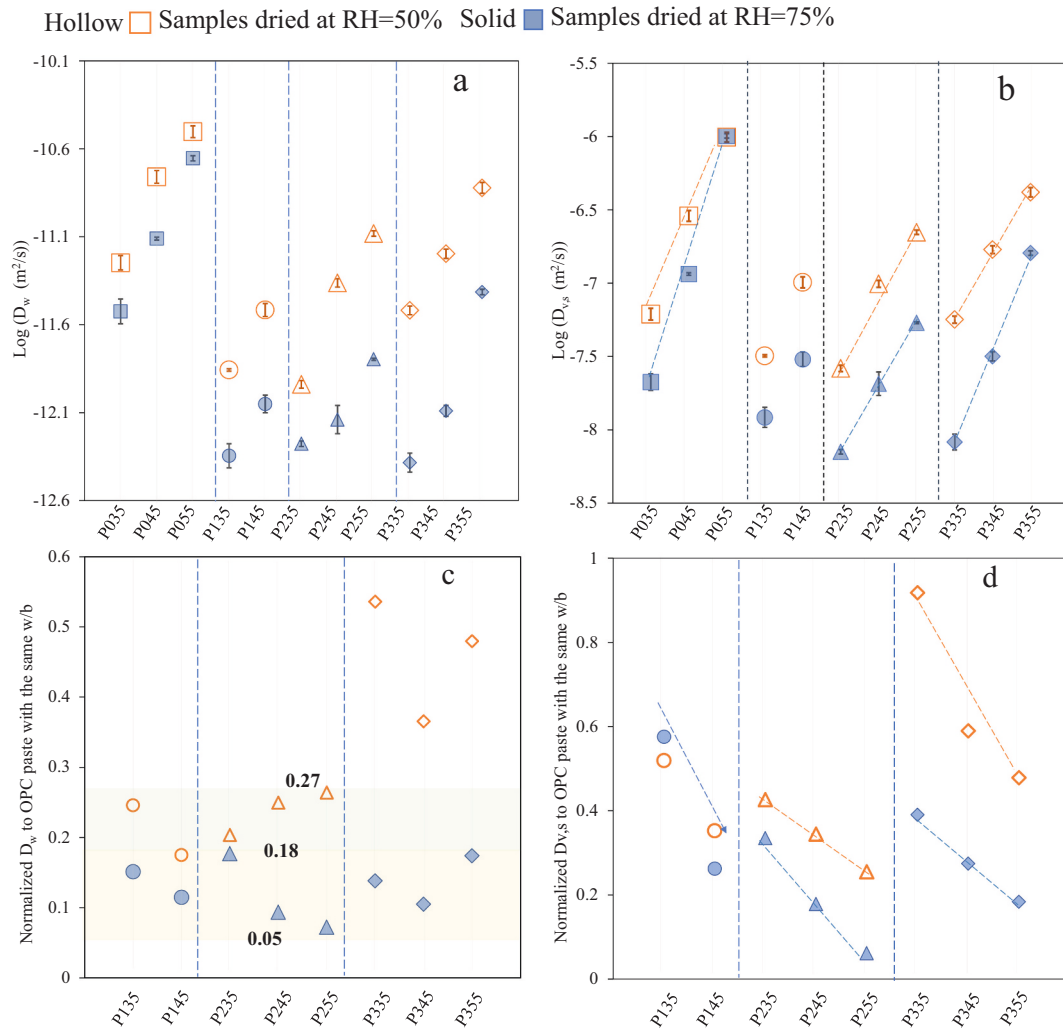
Hollow ☐ Samples dried at RH=50%   Solid ■ Samples dried at RH=75%

Fig. 2. The D_w and $D_{v,s}$ of pastes during drying at RH = 50 % and 75 % (20 °C): a - D_w of all pastes; b - $D_{v,s}$ of all pastes; c - D_w of the blended pastes normalized to the OPC pastes with the same w/b; d - $D_{v,s}$ of the blended pastes normalized to the OPC pastes with the same w/b.

higher moisture capacity than OPC at RH higher than 50 %. The logarithm of $D_{v,s}$ shows an almost linear increasing trend with respect to w/b. The SL binary pastes have the lowest normalized factor with a range of 0.06–0.33 in 50 % RH and 0.25–0.43 in 75 % RH compared to the other pastes with the same w/b. The normalized factors of the FA pastes stay in 0.26–0.58. The factors of ternary pastes are around 0.18–0.39 at 50 % RH, which is a little higher than SL binary pastes. It increases greatly up to 0.92 (close to OPC) in P3 with w/b of 0.35 when drying at 75 %. As the w/b increases to 0.55, this value decreases to 0.47. The decreasing trend of the normalized factor with w/b can be observed in all the blended pastes. It means that the reducing effect of SCMs on vapor diffusion will be magnified at a higher w/b. The higher w/b produces more water in capillary pores for the later age hydration of SCMs [42], so that the pore refinement effect from hydration is more evident resulting in a lower normalized factor of $D_{v,s}$.

3.2. Vapor diffusion coefficient in different RH intervals

A long time is required to reach an equilibrium of the moisture content in cement-based materials for applying Eq. (8). The measurement on the steady-state flux through discs is a more popular method to determine the vapor diffusivity in cement-based materials than the semi-infinite drying method. We referred to the ASTM E96/E96M-13 [28] standard and created the tube setup for the D_v test (Fig. 1). Fig. 3 provides some typical data during the experimental process. Both the temperature and RH were controlled well with a stable value (Fig. 3a). The effect of leakage from dummy samples was evaluated by normalizing the difference in D_v with and without consideration of leakage to D_v value. Fig. 3b presents the typical results, illustrated with P035 at four intervals, and it shows that the leakage induces a 4 % deviation in the stable state D_v value (after about 180 days). It should be noted that all the "D_v" values in the figures are the average diffusion coefficient at a certain RH interval (namely, $\overline{D_v}$). Fig. 3c shows the evolution of $\overline{D_{v,t_i}}$ for pastes with $w/b = 0.35$ in two RH intervals. The samples, including those that are not shown in Fig. 3c, reached a steady state flux after 32 days except P035 in 97.6 %–75.5 % intervals. $\overline{D_v}$ of P035RH97–75 continued to increase until 183 days, and this phenomenon exists in all the three parallel tubes (see the decreasing slope of the weight loss in

Fig. S2-a in supplementary information).

The $\overline{D_v}$ at about 182 days is plotted in Fig. 4 as the indication of the steady-state diffusion coefficient. The increase in the RH intervals tend to increase the deviation within the 3 parallel tests, which is consistent with the results of the cup methods in [19]. However, the deviation level in the tube method is lower than in the cup method. It is due to not only the better sealing of tube method but also the differences in mixtures and disc size compared to the test in [19]. Overall, the tube method for measuring the vapor diffusivity is at least as valid as the traditional cup methods.

Fig. 4a illustrates the $\overline{D_v}$ of pastes with w/b of 0.35 in four different RH intervals. The FA binary paste (P135) has the lowest $\overline{D_v}$ with a value of only half of that in P035 when the RH interval is lower than 80 % (85 % to 75 %). In RH75-50, the SL binary paste has the highest $\overline{D_v}$. The discrepancy in coefficient value between the blended pastes and OPC pastes increases after this RH interval because the $\overline{D_v}$ in OPC pastes has an evident increase after this RH but the $\overline{D_v}$ in the blended pastes seems to be moisture independent with only minor changes in the four RH intervals. This is consistent with the results reported in the previous investigations [19–21]. However, if we analyze the details of the diffusion coefficient of the blended pastes in different RH intervals, we can see that it is not completely RH independent. With a $w/b = 0.35$, the $\overline{D_v}$ of the ternary paste decreases slightly as the RH intervals increase, and that of the SL binary paste has an increase after RH85-75. The decreasing trend in $\overline{D_v}$ is still observed in the FA and ternary pastes with w/b of 0.45 (Fig. 4b) as the RH goes to a higher level. The reduction effect from SCMs on the vapor diffusion is more evident at the higher w/b (from Fig. 4a to c) in RH intervals higher than 62.8 % (75.5 % to 50 %). For instance, the $\overline{D_v}$ of SL blended paste normalized to OPC paste is 0.52, 0.29 and 0.14 for w/b of 0.35, 0.45 and 0.55, respectively, which is similar to the findings in the semi-infinite drying test ($D_{v,s}$). The further blending of LL increases the moisture diffusion in pastes below the RH interval of 97.6 %–50 %, but the differences in the SL binary and ternary pastes are negligible after this interval. The logarithm of $\overline{D_v}$ almost has a linear correlation with w/b. A change in w/b from 0.35 to 0.55 brings an increase in the coefficient of SL blended and OPC pastes with a factor about 2.5 and 10, respectively (Fig. 4d). It is much lower than the increase in $D_{v,s}$ from semi-infinite drying test (Fig. 3b). A further comparison between $D_{v,s}$
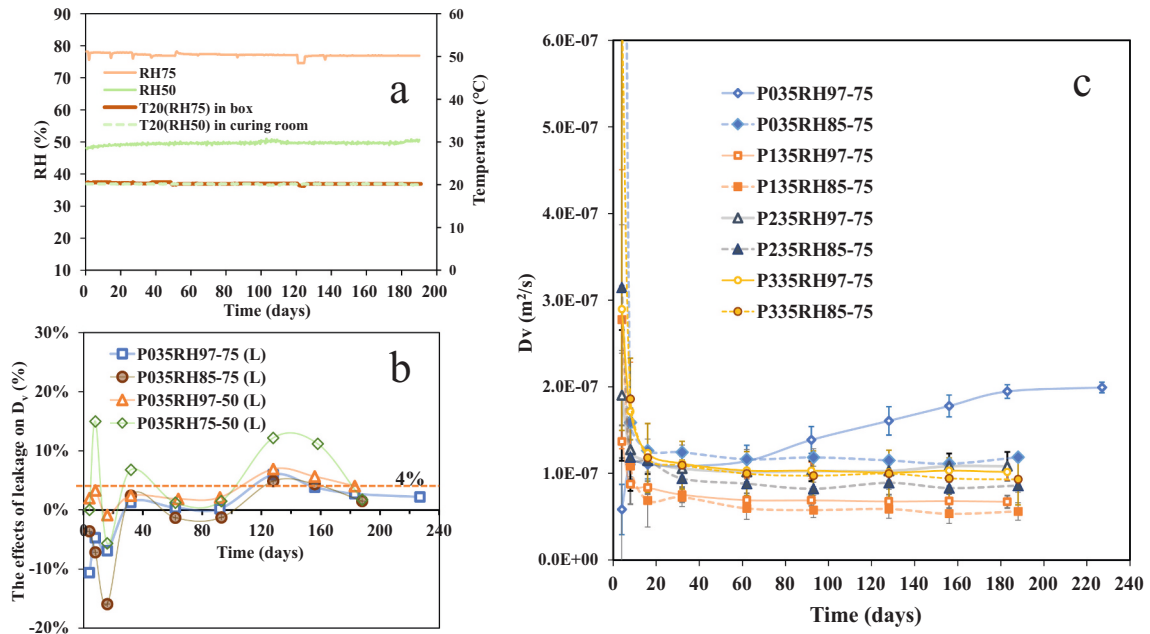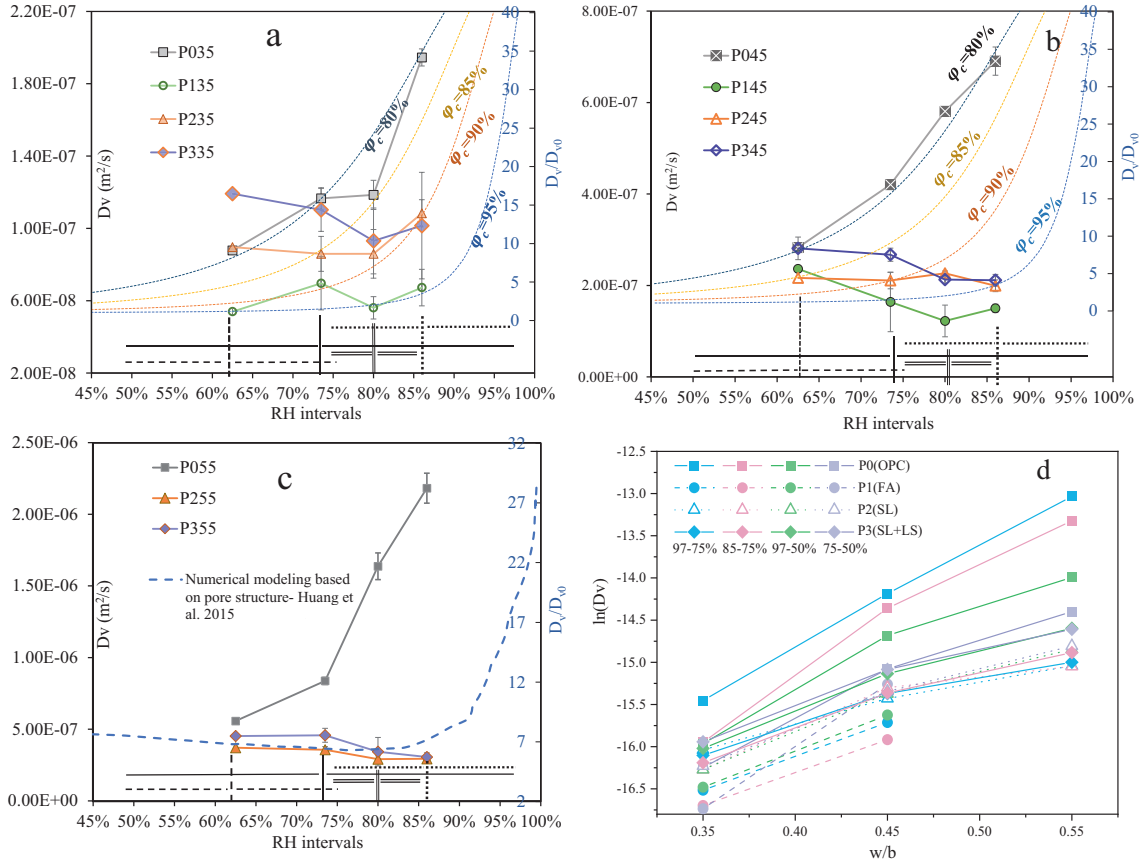

Fig. 3. Some typical data during the vapor diffusion coefficient test. a - the conditioning temperature and RH monitored by testo 174H sensor. b - the effect of leakage normalized to the value of D_v. c - the typical evolution of vapor diffusion coefficient versus time. Note that D_v in the figure is $\overline{D_v}$ in the text.

Fig. 4. $\overline{D_v}$ of all the pastes in 4 RH intervals. a - pastes with $w/b = 0.35$; b-pastes with $w/b = 0.45$; c - pastes with $w/b = 0.55$; d - comparison between different w/b. The evolution of D_v/D_{v0} calculated with Eq. (14) is also plotted in a and b with 4 different critical RH ($\varphi_c = 80$ %, 85 %, 90 %, and 95 %). A typical numerical modeling result is adopted in c from [23].

and $\overline{D_v}$ will be discussed in the last section.

Some publications focused on the relationship between the vapor diffusion coefficient and the RH or saturation condition in cement-based materials. For the blended mortar, the vapor transport properties seemed to show a minimal dependence on the RH when the data of OPC and blended mortar were plotted in the same figure [20]. However, there is an increase in $\overline{D_v}$ when RH goes to a rather high level (97.6 % to 94.6 %) in both adsorption and desorption process as presented in different figures in [19]. The modelled results [4,23] indicate that the D_v of the condensable vapor in porous concrete is apparently dependent on the RH or saturation condition. Because the pores will be gradually filled by the liquid from small to large size as the RH increases, the free path for the vapor diffusion will be blocked by liquid and the moisture transports with a mix of vapor diffusion and liquid flow.

The non-saturated pore walls are covered with an adsorbed water layer, whereas the empty pores are filled with a dry air and water vapor gas mixture [43]. As described in detail by Baroghel-Bouny [2], the moisture transport in cement-based materials involves the transport of both the gas (vapor) and liquid phase under non-saturated conditions when the pore volume is only partially filled with the liquid phase. Depending on the considered material and on its saturation state, either process can be prominent. Before the liquid phase reaches a contiguous connection (percolation) at the critical RH condition (φ_c), the vapor diffusion dominates the moisture transport process. Otherwise, the Darcian moisture transport of the liquid phase is prominent, and in this case, particularly high values of the transport coefficients are expected. Therefore, the results from the cup method will overestimate the vapor diffusion at the high RH interval due to the mixing of liquid flow; this phenomenon is evident in OPC pastes (see Fig. 4).

An empirical formula was proposed by Bazant and Najjar [43] to describe the dependence of the moisture transport coefficient on RH, which was modified into Eq. (14) by Sakata [44].

$$\frac{D_v}{D_{v0}} = 1 + \frac{\frac{D_s}{D_{v0}} - 1}{1 + \left(\frac{1-\varphi}{1-\varphi_c}\right)^n} + (\varphi - 1)\frac{\frac{D_s}{D_{v0}} - 1}{1 + \left(\frac{1}{1-\varphi_c}\right)^n} \tag{14}$$

where D_v, D_s, and D_{v0} are the vapor diffusion coefficients in the cement-based materials with RH= φ, 1, and 0, respectively. Actually, D_s is the transport coefficient of the liquid calculated based on the gradient of the vapor content. The n is an empirical exponent constant. The results of this formula were in good agreement with the simulation results based on a pore network model in [4] involving both the vapor diffusion and liquid flow. Eq. (14) was used to explain the difference in the dependence of $\overline{D_v}$ on RH condition. $D_s/D_{v0} = 50$ was selected as the typical value for the OPC-based concrete with w/b of about 0.45 based on both experimental results and simulations [4,19,20,23]. $n = 2$ was used as a general value according to the previous analysis based on the extended percolation theory in [35]. Fig. 4a and b include the evolution of D_v/D_{v0} in pastes with different critical percolation points ($\varphi_c = 80$ %, 85 %, 90 % and 95 %). It shows that the tendency of OPC pastes is really close to the modelled evolution at $\varphi_c = 80$ %–85 %, and that of the blended pastes is similar with the modelled results at $\varphi_c = 95$ %. This means that the percolation of the liquid in OPC pastes occurs under a much lower saturation state than that of the blended pastes, which is consistent with our previous results [35]. It implies that the different percolation point of the liquid in pastes may be the main reason for the large discrepancy in dependence of the $\overline{D_v}$ on RH for different binder systems. Based on the

modeling investigation [23], the mild decrease in $\overline{D_v}$ with the elevated RH may be due to the blocking of the vapor transport without boosting of the liquid flow (Fig. 4c).

3.3. Chloride migration coefficient

The chloride migration coefficient is another important mass transport parameter in cement-based materials that is related to the durability of reinforcement concrete. Fig. 5 demonstrates the migration coefficient tested by the RCM method (D_{RCM}) at curing ages of 28 and 90 days. In both OPC and binary pastes, the trend is, as expected, that the D_{RCM} increases as the w/b increases. However, the influence from w/b is much weaker in the ternary system with a replacement of OPC by 51 % SCMs compared to the others.

The blending of SCMs evidently reduces the D_{RCM} of pastes with w/b higher than 0.45 at 28 and 90 days. With a $w/b = 0.35$, the FA blended paste has a higher D_{RCM} than OPC with a normalized value of about 1.1 at 28 days, but the normalized value descends to 0.39 at 90 days (see Fig. 5b). The normalized value of P235 and P335 is about 0.7 at 28 days, which is close to the value of P145. The reducing effect of SCMs on D_{RCM} becomes more significant in pastes with a higher w/b. This phenomenon is similar to the findings on moisture transport (Fig. 2d and 4). Pastes have a lower D_{RCM} at 90 days than at 28 days except for OPC with $w/b = 0.55$ (P055). The chloride migration coefficient is a time-dependent parameter that will decrease with the curing time following an empirical power function [13,45–47] due to the continuous hydration. However, an interesting deviation similar to P055 was detected in the previous investigations [46,47] as well. The OPC based concrete might have a higher chloride migration coefficient at later age when the w/b is rather high (> 0.5). Because of the increase in the hydration degree of

Fig. 5. Chloride migration coefficient of pastes tested by RCM. a - the original value; b - the value of blended pastes normalized to OPC with the same w/b.

SCMs, the normalized value decreases from 28 to 90 days and the value of FA binary pastes has the most evident change. The blended pastes have the normalized value at a much lower value range at 90 days (from 0.5 to 0.1) than at 28 days (from 1.1 to 0.3).

3.4. Structure of pastes

3.4.1. Pore structure by MIP

The MIP measurement was used to investigate the pore structure in hardened cement-based materials. Pore size measured by MIP refers to the threshold diameter corresponding to the intruded pressure rather than a real size, which will underestimate the size of big pores within the "ink-bottle" shape [48,49]. Therefore, it should be noted that the pore size in this text represents not only the diameter of cylinder pores but also the neck of "ink-bottle" pores that influence the transport properties as well. However, it can provide the threshold diameters and intrudable pore space as the comparative indices for the pore information in cement-based materials [22,48]. Fig. 6 presents the differential pore size distribution of pastes and the detailed comparison between different categories. The intrudable pore volume has been classified into three ranges: mesopores (4.5–50 nm), middle capillary pores (50–100 nm) and large capillary pores (>100 nm) [50]. The percentage of the intruded pore volume in these three ranges is illustrated in Fig. 7. The CP is the inflection point on the curve of intruded volume versus pore size, such as the pore size corresponding the peak value in the dV/dlog(D) curve [22].

Fig. 6a and b show that the blending of FA decreases the CP of pastes with w/b of 0.35 and 0.45 under the sealed curing condition after 390 days. However, SL brings an increase in the CP of pastes with w/b of 0.35 and 0.45 under the seal curing. Therefore, the much lower $\overline{D_v}$ (Figs. 2 and 4) of the blended pastes can hardly be ascribed to the reduction in the CP that was mentioned as the main factor controlling the moisture transport in [20,21]. SL could decrease the CP of pastes at later age when the pastes were cured in water [9]. Water curing provides sufficient water in the big capillary pores so that the precipitation of the hydration products can fill these pores during later hydration of SL. However, during the sealed curing (without the water supply), the inner RH of the pastes is no >95 % after 7 days even with the dilution effect from 50 % SCMs [51]. According to Kelvin's equation, liquid water can only be accessible in pores with a diameter smaller than 70 nm in 95 % RH at 20 °C when the effect from alkali ions has been taken into account [6]. Consequently, the filling effect from the hydrates produced by the later age hydration of FA and SL can only occur in the mesopores and middle capillary pores under the sealed curing condition (as in this study). This may explain why in Fig. 6, the volume of the pores with a size (or neck size) < 100 nm in the blended pastes is significantly lower than that in OPC, whilst there still exists a certain amount of large capillary pores (> 100 nm) in the blended pastes, especially for those with w/b of 0.35 and 0.45. It might also be the reason for the differences in the effects of SL on the CP between the water curing in [9] and the sealed curing in this study. Although the total porosity (6 nm–373 μm) in FA binary pastes is higher than that in OPC pastes, the main differences are in the volume of intrudable pores smaller than 100 nm. In both conditions with w/b of 0.35 and 0.45, the FA blended pastes have the similar large capillary pore volume but a much higher mesopores volume compared to OPC (see Fig. 7). The volume of the middle capillary pores decreases after the blending of FA due to its secondary hydration at the later ages, and this effect is prominent in pastes with w/b of 0.45 (Fig. 6b and Fig. 7).

The total porosity (6 nm–373 μm) of SL binary pastes with w/b of 0.35 and 0.45 is close to that of OPC with the same w/b, but the increase in the volume of mesopores pores with meso-neck occurs after the blending of SL. A reduction in the percentage of middle and large capillary pores can be observed in SL binary pastes with w/b of 0.45 and 0.55 compared to OPC pastes (Fig. 7). It should be noted that this unnecessarily implies a high reduction effect in the actual size of the pore,
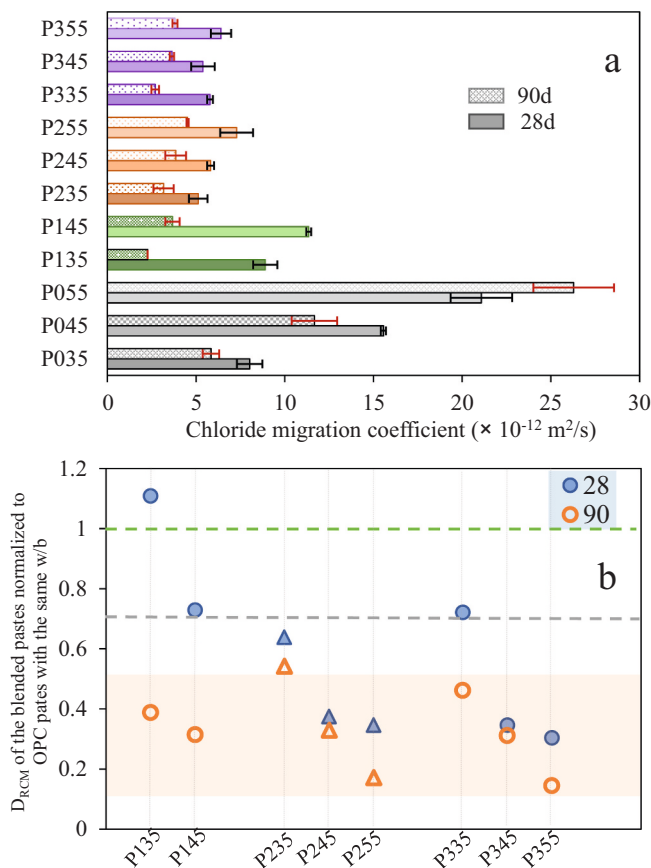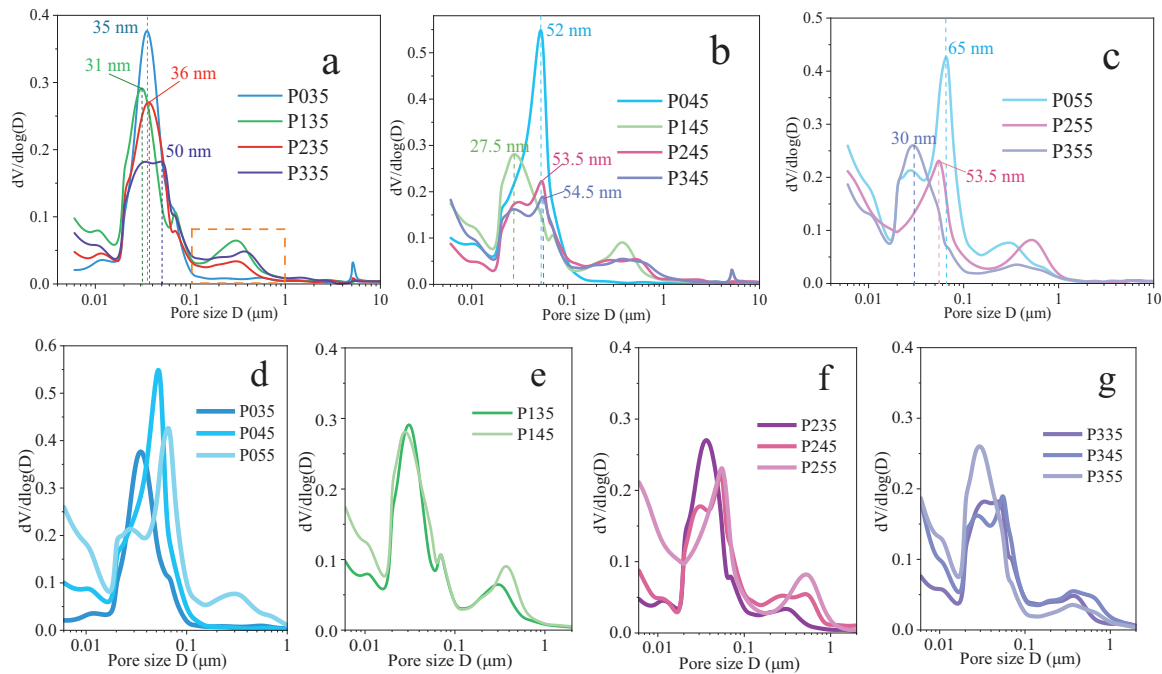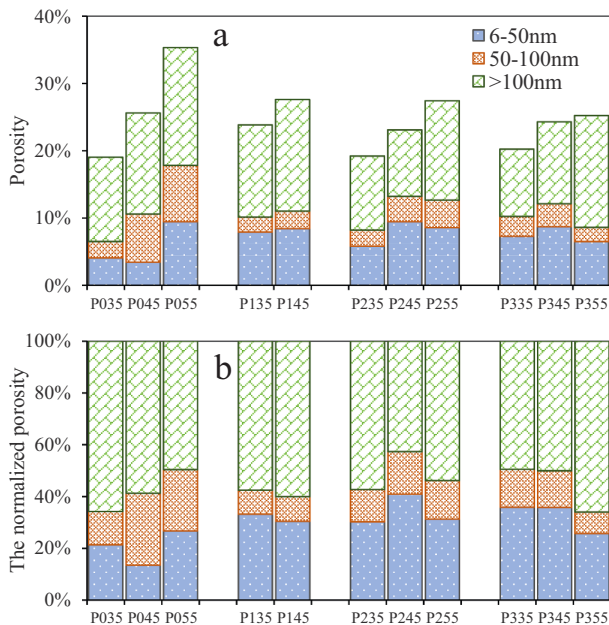
Fig. 6. Pore size distribution of pastes measured by MIP: the comparison between pastes with *w/b* of 0.35 (a), 0.45 (b), and 0.55 (c); comparison between different *w/b* for OPC (d), the FA blended (e), the slag binary (f), and ternary (g) pastes.

Fig. 7. Intrudable pore size distribution of pastes tested by MIP: a - original value; b - the percentage of the intruded pore volume normalized to 1.

since it may also result from an increase in the percentage of "ink-bottle" pores with small necks. Moreover, the latent hydraulic reaction of SL may happen on the local surface of large capillary pores to produce hydrotalcite-like phase, C-A-S-H gel and Ca—Al layered double hydroxide phase [52], resulting in a reduction in the pore sizes as well as the pore volume. Although the LL in ternary pastes alters the phase composition in the hydration products [53], its effect on the pore structure is very weak in pastes with *w/b* of 0.35 and 0.45. The dilution effect of LL introduces a higher effective water to hydraulic binder (OPC and SL) ratio, so it increases the percentage of mesopores in the ternary

paste compared to the SL binary paste with *w/b* of 0.35. With the *w/b* of 0.55, the CP in the SL binary pastes is slightly lower than that of OPC (Fig. 6c). A further replacement of LL increases the volume of the large capillary pores but decreases the CP from 53.5 nm in binary pastes to 30 nm in ternary pastes.

Pastes with the higher *w/b* have a higher total porosity (see Fig. 7). The change in *w/b* from 0.35 to 0.45 causes an evident increase in the CP of OPC pastes from about 35 to 53 nm, and OPC with *w/b* of 0.55 has a CP up to 65 nm. The effect of *w/b* on the CP in the blended pastes is more complex than the effect on OPC. The increase in *w/b* even decreases the CP in the FA blended pastes, and the same trend can be observed in the ternary pastes. The volume of large capillary pores typically increases with the increase in *w/b* in all binder systems, but the changes in mesopores and middle capillary pores is dependent on the binder type.

3.4.2. Pore structure parameters from electrical conductivity

As shown in Eq. (1), the pore structure parameter related to the mass transport process can be detected by the electrical conductivity of the paste and its pore solution. However, the conductivity of the actual pore solution is difficult to experimentally measure. Rajabipour and Weiss [54], and Wilson et al. [27] used the solution extracted from the hardened pastes to measure the electrical conductivity of the pore solution. The problem with this method is that it neglects the conductivity of ions accumulated in the diffusion layer between the solid surface and the solution. The superficially trapped ions may be difficult to be extracted by squeezing of the pore solution [55]. Omitting of the surface conduction would underestimate the *FF* in the porous structure as mentioned in [54,56], and it is very significant when the conductivity of electrolyte (pore solution) is not so high (<5 S/m) [57]. An alternative way to determine the ionic conductivity of pore solution is to calculate the value based on the concentration of highly conductive ions in the pore solution derived from the degree of hydration, binder chemical composition, and alkalis binding to the cement hydration products [58]. It seems to be more plausible to take all the highly dissolvable alkalis into account, which roughly includes the conductivity of ions trapped in the diffusion layer.

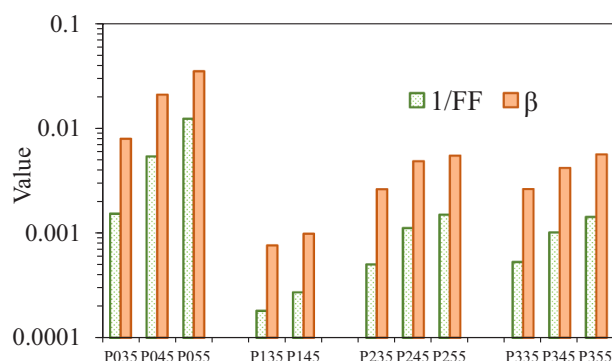Table 4 presents the measured values of the electrical conductivity of

Table 4

The measured electrical conductivity of pastes, the calculated conductivity of the pore solution, the inverse of *FF*, porosity by MIP and pore connectivity in pastes at about 1 year (390 days).

Sample	Electrical conductivity (mS/cm)		1/*FF*	*Φ*	*β*
	Paste	Pore solution			
P035	0.251	165.9	1.52E-03	0.19	7.84E-03
P045	0.701	131.3	5.34E-03	0.26	2.07E-02
P055	1.249	102.9	1.21E-02	0.35	3.45E-02
P135	0.019	104.4	1.78E-04	0.24	7.48E-04
P145	0.026	96.0	2.71E-04	0.28	9.82E-04
P235	0.075	149.6	4.98E-04	0.19	2.60E-03
P245	0.128	114.5	1.12E-03	0.23	4.85E-03
P255	0.167	111.6	1.50E-03	0.27	5.46E-03
P335	0.070	133.3	5.26E-04	0.20	2.60E-03
P345	0.085	86.9	9.75E-04	0.24	4.01E-03
P355	0.111	78.0	1.42E-03	0.25	5.60E-03

Table 5

The calculated inverse of *FF* of pastes at 28, 90 and 365 days.

Sample	1/*FF*		
	28 days	90 days	365 days
P035	3.09E-03	2.46E-03	1.52E-03
P045	6.88E-03	6.21E-03	5.34E-03
P055	1.19E-02	1.21E-02	1.21E-02
P135	2.97E-03	5.41E-04	1.78E-04
P145	5.65E-03	1.01E-03	2.71E-04
P235	1.28E-03	9.07E-04	4.98E-04
P245	2.41E-03	1.65E-03	1.12E-03
P255	3.73E-03	2.22E-03	1.50E-03
P335	1.44E-03	8.87E-04	5.26E-04
P345	2.34E-03	1.58E-03	9.75E-04
P355	3.51E-03	2.27E-03	1.42E-03

the pastes, the conductivity of the pore solution, the inverse of *FF* (1/*FF*), porosity and pore connectivity. The conductivity of the pore solution was calculated by the empirical function in [35], which involves the chemical composition of the binder and the degree of hydration (evaporable water content) at the corresponding hydration time. The calculated conductivity of the pore solution in pastes ranges from 165 to 78 mS/cm. Apparently, the blending of SCMs decreases the conductivity of pore solution mainly due to the lower content of dissolvable alkali in SCMs compared to OPC [59] and the dilution effect of SCMs leading to an increased effective *w/b*. The increase in *w/b* from 0.35 to 0.55 in the OPC paste induces the highest increase in the 1/*FF*, with a factor of about 8 times compared to the blended pastes and with the maximum factor about 3 times in the SL binary pastes.

Fig. 8 shows that the pore connectivity (*β*) is the same as 1/*FF* in terms of its tendency to change with respect to the change in *w/b* and the binder types. A significant increase in both 1/*FF* and *β* can be observed as the *w/b* increases. The blending of FA has a huge reduction effect on the 1/*FF* with a factor of about 1/8.5 and 1/20 in the paste with *w/b* of 0.35 and 0.45 normalized to OPC, respectively (see Table 4 and Fig. 8). SL induces a normalized factor of about 1/3, 1/5, and 1/8 in the 1/*FF* of pastes with *w/b* of 0.35, 0.45, and 0.55, respectively, compared to OPC with the same *w/b*. The ternary pastes with LL (P3-series) have a similar 1/*FF* or *β* as the SL (P2-series) binary pastes. Table 5 presents the 1/*FF* of pastes at 28, 90 and 365 days, which was calculated based on the data in Table S3 (see supplementary information). 1/*FF* decreases as the hydration proceeds from 28 to 90 days due to the structural growth of the hydration products and the consumption of evaporable water. This change is more evident in the blended pastes compared to OPC, especially in the FA blended pastes in which the secondary hydration of FA occurs at the later ages [35,42].

Fig. 8. The inverse of *FF* and pore connectivity of pastes cured for 1 year.

4. Discussion

4.1. The refinement effect of SCM on the pore structure

SCMs have an impact on the pore structure in cement-based materials. Their refinement effect on the CP in pastes depends on the curing conditions. The water curing condition supplies abundant water for the later hydration to precipitate the hydration products in the large capillary pores, so that the latent hydraulic reaction of SL can decrease the CP in pastes [9]. When the pastes are cured under the sealed condition, SL presents no such effect on the CP as shown in Fig. 6, due to the lack of water in the large capillary pores. Nonetheless, SL decreases the percentage of large capillary pores and increases the percentage of mesopores or pores with mesoscale neck in the pastes with *w/b* of 0.35 and 0.45. It can even reduce the total porosity (6 nm–373 μm) in pastes with *w/b* of 0.55 (see Fig. 7). Therefore, it can induce a significant reduction in the 1/*FF* and *β* of the blended pastes (see Fig. 8). FA has an evident reduction effect on the CP in the hardened paste at a later age (after 390 days curing), but this effect is weak before 90 days even under a water curing condition [9,22]. It increases the percentage of mesopores or "ink-bottle" pores with a mesopore size neck, which shows an increase in the volume of mesopores in the MIP test (see Fig. 7 and results in [22]). Moreover, the unreacted FA may also act as an impermeable "aggregate" as shown in the SEM images in [9,60]. The combined effects contribute to the increase in the tortuosity and decrease in the pore connectivity (see Fig. 8). A further blending of LL in slag pastes seems to have no significant influence on the pore size distribution, so that the SL binary and ternary pastes with the same *w/b* have minor differences between their 1/*FF* and *β*. A higher *w/b* provides more water accessible for the later age hydration so that the refinement effect from SCMs becomes more evident at higher *w/b* (see Figs. 6–8), thus resulting in an increase in the reduction effect on the moisture or chloride transport coefficient (see Fig. 2d, 4, and 5b).

The transport of moisture and ions in the cement-based materials is not only related to the pore structure but also the chemical structure of the hydration products. However, there still exists many undetectable details in the pore structure, such as the volume percentage of stagnant pores (dead-end pores) in which the mass transport rate will be much slower than the connected pores [61]. The increase in number of stagnant pores may be detectable under SEM [9,60] within a very small region (micrometer size), but the bulk data at macroscale size is not measurable by any method at present. The increase in the dead-end pores or the decrease in the pore connectivity may be due to the formation of foil-like C-A-S-H in the blended pastes [52,62]. The strengthened interfacial hydrogen bond and indirect adsorption of Cl ions in C-A-S-H slows the water and chloride transport in the nanometer channel compared to C-S-H [63]. A detailed discussion of chemical structure of hydration products and the mass transport properties is beyond the scope of this paper.

4.2. Correlation between moisture transport during semi-infinite drying, tube test and porosity

The previous investigation [64] found that the CP had a correlation with water permeability and the chloride migration coefficient. However, this paper shows that only the $\overline{D_v}$ of OPC pastes increases with the increase in the CP. The correlation between $\overline{D_v}$ and CP is, more or less, arbitrary without any clear correlation in the blended pastes (see Fig. S4 in supplementary information).

The correlation between porosity and conductivity of sedimentary rocks was empirically described by Archie's law [65,66]. The relationship between the *FF* and porosity of the hardened cementitious materials was discovered [26,67], as shown in the following equation.

$$\frac{1}{FF} = a * \phi^n \tag{15}$$

where a is a non-uniform constant, n is the shape factor and ϕ is the volume of the conductive saline solution that corresponds to the volume of pores filled with water at 97.6 % RH. Eqs. (16) and (17) can be obtained by substituting Eq. (15) into Eq. (1). Herein, we extend the D_p and D_0 to moisture transport coefficient in the saturated cement-based materials (as liquid) and in the air (as vapor), respectively.

$$\frac{D_p}{D_0} = a * \phi^n \tag{16}$$

$$log D_p = log a D_0 + n log \phi \tag{17}$$

Fig. 9 shows the correlation between the logarithm of the drying constant (k_w) and the volume of pores with liquid at 97.6 % RH. The average value of k_w for each sample was calculated from data in Table S1 and S3 (Supplementary information). The critical Kelvin's diameter for the condensation of vapor into pore water is about 150 nm at 97.6 % RH [6]. Therefore, the porosity of pores smaller than 150 nm (from data in Fig. 7) is plotted in Fig. 9. There are only two samples that deviate from the regression line (see the circled markers in Fig. 9). This may be due to the fact the percentage of ink-bottle pores in P145 and P255 is much higher than that in the other samples, as mentioned in the previous section. Apart from the two points, a good linear regression can be observed between log (k_w) and log (ϕ) for the sample drying at both 50 % and 75 % RH, which is consistent with the formula in Eq. (16). Because of the big difference in the moisture capacity as well as in the pore solution concentration, there is no general correlation between the porosity and D_w or $D_{v,s}$, as shown in Fig. S5-a and S5-b (in supplementary information). It is apparent that the OPC with *w/b* of 0.35 has the lowest porosity (see Fig. 7), but the D_w or $D_{v,s}$ is the highest among the pastes
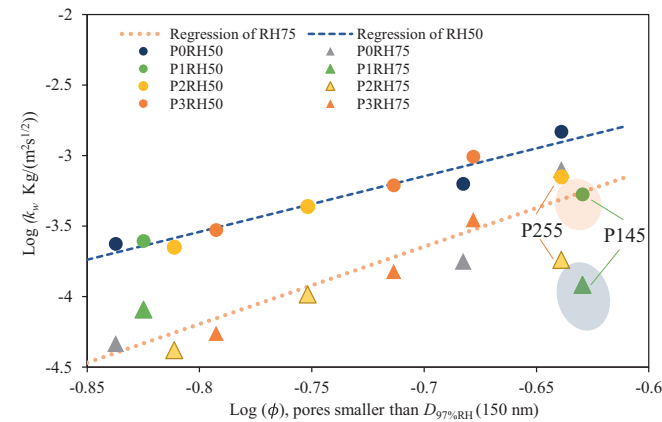
with the same *w/b* (see Fig. 2). SCMs have a significant reduction effect on the pore connectivity in pastes (see Fig. 8) and also modify the structure of hydration products (C-A-S-H) [52,60,63,68]. Their effects on both refining pore structure and chemical structure result in a much slower moisture transport in the blended paste than in OPC pastes even with a lower porosity.

It seems that the log(ϕ) has a better linear correlation with the logarithm of the average vapor diffusion coefficient ($\overline{D_v}$) in RH97-50 or RH75-50 than in RH97-75 or RH87-75 (see Fig. S5-c and d in supplementary information). There are much more data deviating from the general linear line in Fig. S5-c than in Fig. S5-d (Supplementary information). This may be due to the fact that the high RH moisture induces a large percentage of pores filled with liquid, which causes the moisture transport process to be strongly mixed with the liquid flow and its blocking effect on vapor diffusion [4]. Consequently, the connectivity of pores determines the moisture transport process instead of the porosity.

Fig. 10 presents the correlation between $\overline{D_v}$ from the steady-state vapor diffusion test (Fig. 4) and $D_{v,s}$ from the semi-infinite drying test (Fig. 2). The value of $\overline{D_v}$ in the RH97-50 is close to the value of $D_{v,s}$ during drying at 50 % RH (linear slope of 0.92 and R^2 of 0.96). However, the difference in D_v and $D_{v,s}$ is more evident at the high RH condition (see Fig. 10b). Due to the data point on the upper right corner (from P055), the R^2 value of data in Fig. 10b is similar with that in Fig. 10a, but it is obvious that the confidence level is very low in correlation at 75 % RH. The correlation also becomes weaker in the blended pastes (see the enlarged part), and the slope becomes much higher compared to the data in Fig. 10a. In one report from Nilsson [30], the $\overline{D_v}$ in the RH interval of 85–60 % is comparable with $D_{v,s}$ during drying at 50 % RH, which is consistent with our result in Fig. 10a. However, the difference between $\overline{D_v}$ and $D_{v,s}$ largely increases at the high moisture level (>75 %). According to the previous investigations [32,69,70], this is mainly due

Fig. 9. The correlation between the drying constant (k_w) and the volume of pores with diameter smaller than the critical Kelvin diameter at 97.6 % RH (150 nm).
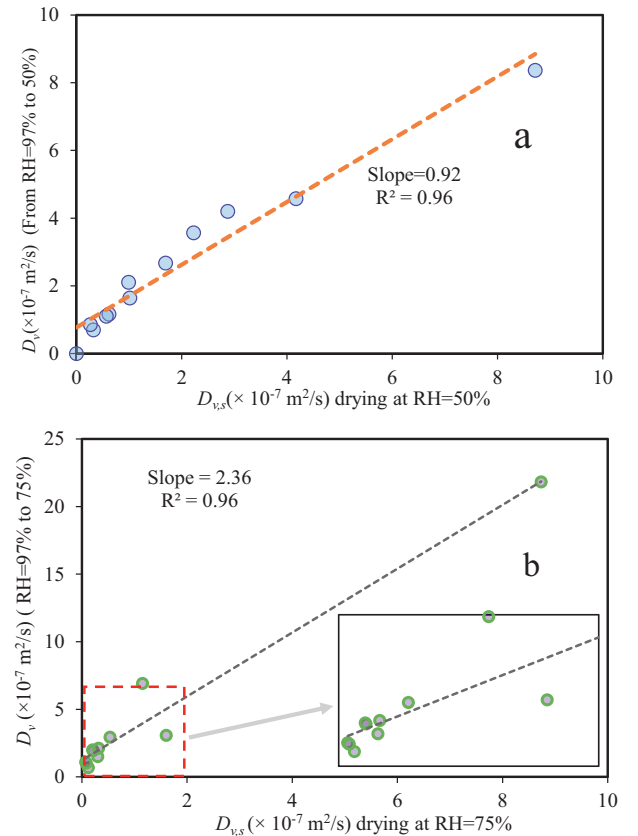

Fig. 10. The correlation between the average vapor diffusion coefficient (D_v) and $D_{v,s}$ from semi-infinite drying at 50 % RH (a) and 75 % RH (b).

to the contraction of C-S-H gel during drying, resulting in the anomalous transport phenomenon. Fick's law can not describe the whole drying process under this kind of non-steady state.

4.3. Correlation between D_v and FF

The moisture transport in cement-based materials also relates to the *FF* and the pore connectivity. Moradllo et al. [71] found that the water adsorption rate correlated to the *FF*, and it was a linear relationship between the initial rate of water absorption and the reciprocal of the square root of the *FF*. The $\overline{D_v}$ of cement-based materials is moisture dependent [19,20], owing to the fact that the liquid will gradually occupy the pores in the structure with the increase in the RH. The increasing RH or saturation condition mixes the vapor diffusion with the liquid flow during the moisture transport process [4,23]. Therefore, the correlation between $\overline{D_v}$ in different RH intervals and $1/FF$ is separately plotted in Fig. 11a-f.

According to the analysis in the previous section, the $\overline{D_v}$ at a high RH interval is determined by the pore connectivity instead of the porosity. A good linear correlation between $\overline{D_v}$ in RH97-75 with $1/FF$ (see Fig. 11a) confirms this conclusion. The enlarged plot in Fig. 11b shows that this linear correlation is general in both OPC and the blended pastes with $R^2 = 0.985$. Because the pore connectivity determines the moisture transport process, the vapor diffusivity of the blended pastes is much lower than OPC pastes at the high RH interval. Although they have a similar porosity (see Fig. 7), the β or $1/FF$ of the blended pastes is much smaller than that of OPC pastes (see Fig. 8).

Fig. 11c indicates that the correlation between the $1/FF$ and $\overline{D_v}$ still exists in RH85-75, but the correlation in the blended pastes deviates from the general trend with a higher slope than the general line as shown in Fig. 11d. The critical RH (φ_c) for the percolation of the liquid in the

blended pastes is much higher than that for OPC (see Fig. 4) due to the difference in pore structure and alkali concentration in the pore solution [35,58]. Therefore, the condition of RH85-75 is sufficiently higher than φ_c for the percolation of the liquid in OPC pastes but it does not reach the level of percolation of liquid in the blended pastes. As the RH intervals decrease, the connectivity of the liquid phase in the pores evidently decreases so that the moisture transport process turns to be mainly determined by the porosity in pastes (see Fig. S5-c in supplementary information). Consequently, the $\overline{D_v}$ of the blended pastes is close to that the OPC pastes with the same *w/b* in RH75-50 (see Fig. 4), even though the $1/FF$ or β of the blended pastes is much lower than that of the OPC paste. The slope of the blended samples in Fig. 11d-f increases, as the major determinant of $\overline{D_v}$ transitions from the pore connectivity to the porosity with the decrease of RH. FA pastes with *w/b* of 0.45 deviates from the fitting line of the blended pastes due to its much lower pore connectivity compared with the SL blended pastes with the same *w/b*.

4.4. Chloride migration coefficient and FF

The chloride migration coefficient in the paste correlates to the pore structure parameter *FF* and the migration coefficient in the pore solution as shown in Eq. (1). Wilson et al. [27] presented a detailed discussion on the relationship between the effective chloride migration coefficient (D_{eff}) and the electrical properties of pastes, such as the electrical conductivity of pore solution and pastes, *FF*, or the pore connectivity. They found a general correlation between D_{eff} from their method and the bulk conductivity of pastes. The data of white cement pastes deviated from the general line when D_{eff} was correlated with $1/FF$ or the pore connectivity. It should be noted that in their study, the conductivity of pore solution was measured by extracting the pore solution from pastes. As mentioned in Section 3.4.2, the conductivity of the extracted pore
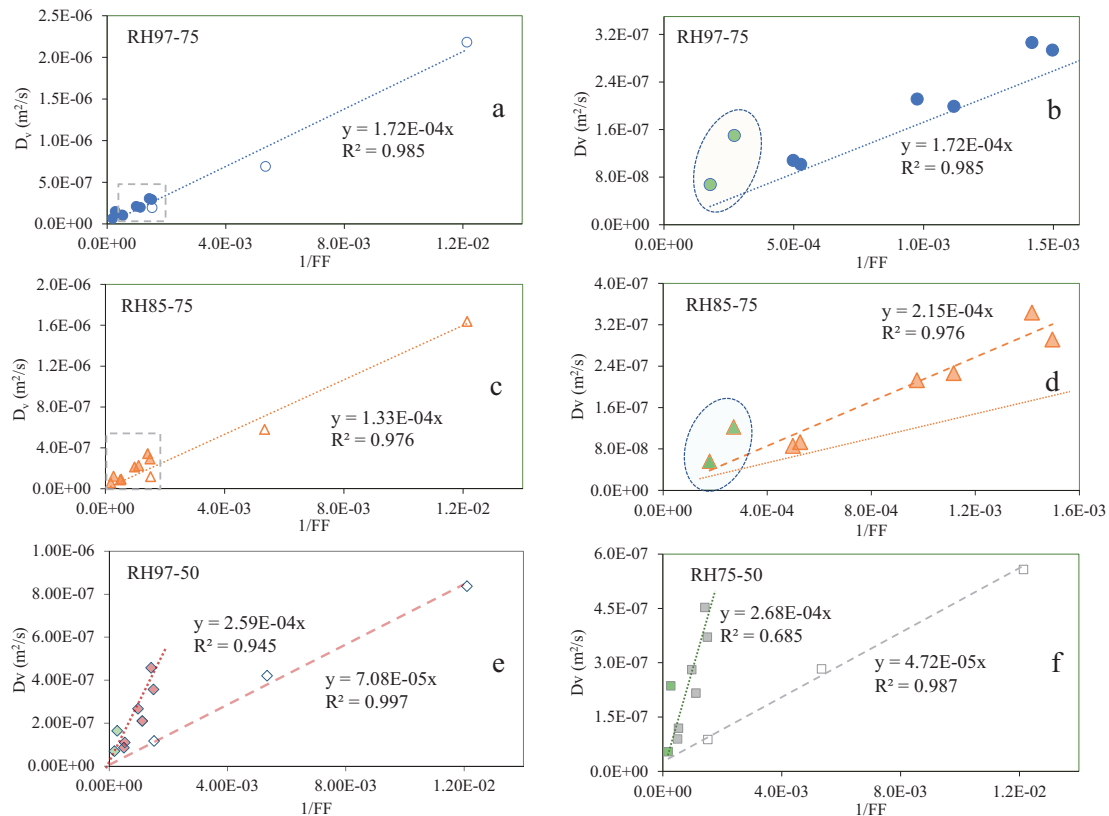
Fig. 11. The correlation between the average vapor diffusion coefficient and $1/FF$: a and b - D_v in RH97-75; c and d - D_v in RH85-75; e - RH97-50; f - RH75-50. The hollow markers are the data of the OPC pastes, the solid markers are the data of the blended pastes, and the green markers are the data of the FA blended pastes. (For interpretation of the references to colour in this figure legend, the reader is referred to the web version of this article.)

solution neglected the surface conductivity, which would impact the calculation of *FF* when the conductivity of the pore solution is low (<5 S/m, such as in LC$_3$ or white cement pastes) [54,56,57]. Moreover, avoiding the carbonation of the extracted pore solution during the whole experimental process is critical for measuring a correct conductivity value for the pore solution because the OH$^-$ (pH) in the pore solution contributes >70 % to the ionic conductivity [35].

Chidiac and Shafikhani [58] developed an effective model to estimate the chloride migration coefficient based on the measured conductivity of concrete and the calculated conductivity of pore solution derived from the binder chemical composition and the hydration degree. Provided that we neglect the binding capacity of the hydration products during the non-steady-state migration of chloride under the applied electric field, Eq. (18) can be used to estimate the D_{RCM} based on *FF*. D_{ps} is the chloride migration coefficient in the bulk pore solution, which was often assumed to be 2.03×10^{-9} (m^2/s) [13], but it could be smaller than this value due to the interaction with other ions in the pore solution.

$$D_{RCM} = \frac{D_{ps}}{FF} \tag{18}$$

Fig. 12 presents the relationship between the measured D_{RCM} (from Fig. 5a) and the *1/FF* (from Table 5). In general, the D_{RCM} of all the pastes is located close to the modelled line (dash line in Fig. 12a), but the pastes with *w/b* of 0.35 deviate from the modelled line when we focus on the low D_{RCM} region (see Fig. 12b). Because the sealed curing pastes were used to measure the conductivity, the pastes with *w/b* of 0.35 are far from the saturation state under this curing condition. However, the D_{RCM} was tested under the nearly saturated condition which might result in a deeper chloride penetration depth or a higher value of D_{RCM}. The conductivity and chloride migration coefficient in [58] was normalized

to the mortar volume and adopted in Fig. 12b. Both the data at 84 days and 1 year stay close to the modelled line. Therefore, the pore connectivity or *FF* should be a key controlling factor for the chloride migration in the OPC based materials.

5. Conclusions

A novel setup and procedure are proposed in this work, which enables to obtain the data of moisture transport coefficients, including k_w, D_w, $D_{v,s}$, and $\overline{D_v}$, within one test procedure. The moisture transport coefficient is dependent on the RH condition due to the condensation of the liquid phase in the pores. SCMs alter not only the moisture transport coefficient at certain RH but also its dependence on the RH condition. The effects of SCMs on the moisture transport properties can mainly be ascribed to their refinement of the pore structure.

$\overline{D_v}$ of OPC pastes presents an increasing trend as the RH increases due to the gradual condensation of water in the porous structure. The φ_c for the percolation of the liquid in cement-based materials is determined by the pore structure and pore solution concentration. The blended pastes have a more complex pore structure and lower alkali ions in the pore solution than OPC pastes; hence the blended pastes require a much higher critical RH for the percolation of the liquid than OPC pastes. It results in a relatively stable $\overline{D_v}$ of the blended pastes in the RH intervals lower than 85 %. An increase in *w/b* augments the reduction effect of SCMs on the moisture transport and chloride ion migration coefficient in the pastes.

FA lowers the CP of pastes after curing for 390 days, but SL has no reduction effect on the CP of the pastes under the sealed curing condition because of the low accessibility of liquid water in large capillary pores. The blending of FA induces an increase in the total porosity but does not increase the volume of the large capillary pores. SL decreases the percentage of large capillary pores and increases the percentage of mesopores or "ink-bottle" pores with a mesoscale neck. Both FA and SL have a large reduction effect on the pore connectivity in the pastes after long-term curing. A further blending of LL has a similar effect but not as big as the SL blended pastes on the pore connectivity in the hardened pastes after about 1 year. The higher *w/b* provides more water for the later age hydration of FA and SL, so that their refinement effects become more evident.

$D_{v,s}$ is close to $\overline{D_v}$ at the low RH condition (~50 %), but the difference between them will largely increase at a high RH. Both the *FF* and porosity of small pores (middle capillary and mesopores) are important parameters that determine the moisture transport properties in the cement-based materials. *FF* is the major determinant for the moisture transport process at a high RH interval, and the porosity of small pores is the major determinant at a low RH interval.

A highly simplified model was proposed with only one measurable parameter *FF* of pastes for the correlation to the chloride migration coefficient. This model can generally estimate the D_{RCM} of both pastes and mortars. Regarding the performance concretes, the blending of SCMs has an impact on pore structure in the interfacial transition zone. Some more detailed investigations are needed to apply the data in this paper into the blended concretes.

CRediT authorship contribution statement

Liming Huang: Conceptualization, Methodology, Investigation, Data analysis, Writing-Original Draft, Writing-Review & Editing. Luping Tang: Methodology, Writing-Review & Editing, Supervision, Project administration, Funding acquisition. Ingemar Löfgren: Investigation, Writing-Review & Editing. Nilla Olsson: Investigation, Project administration. Zhenghong Yang: Review & Editing, Supervision, Project administration. Yongqiang Li: Investigation, Resources.
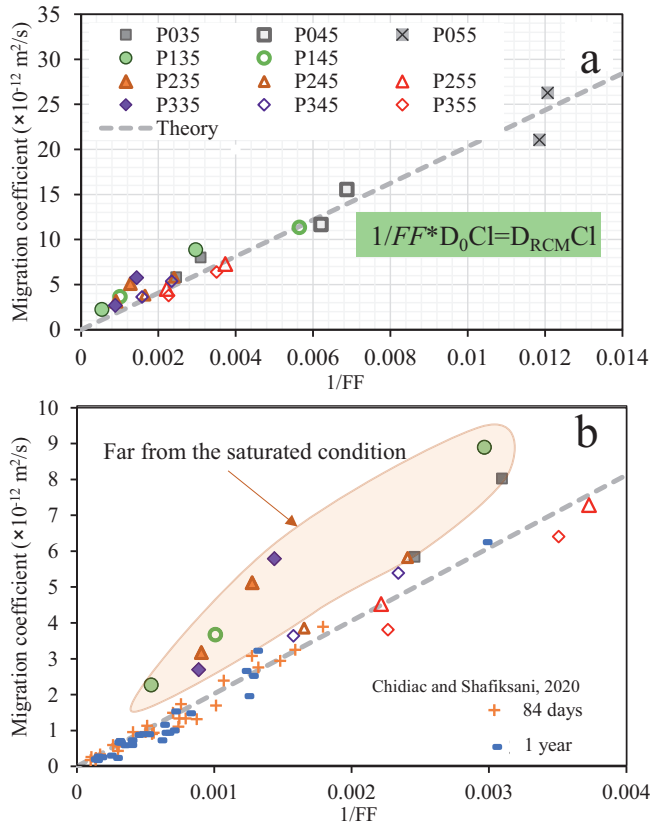
Fig. 12. The correlation between the chloride migration coefficient and *1/FF*: a - data in this paper at the curing time of 28 and 90 days; b - data in [58] was used and adopted after some normalizations.

Declaration of competing interest

We declare no conflicts of interest.

Acknowledgements

Appendix A. Supplementary data

Supplementary data to this article can be found online at https://doi.org/10.1016/j.cemconres.2022.106949.

References

[1] L.-O. Nilsson, Jacobs, Methods of measuring moisture in building materials and structures, Springer, 2018.

[2] V. Baroghel-Bouny, Water vapour sorption experiments on hardened cementitious materials. Part II: essential tool for assessment of transport properties and for durability prediction, Cem. Concr. Res. 37 (2007) 438–454, https://doi.org/10.1016/j.cemconres.2006.11.017.

[3] K. Li, C. Li, Modeling hydroionic transport in cement-based porous materials under drying-wetting actions, J. Appl. Mech. 80 (2013), 020904, https://doi.org/10.1115/1.4007907.

[4] D. Quenard, H. Sallee, Water vapour adsorption and transfer in cement-based materials: a network simulation, Mater. Struct. 25 (1992) 515–522, https://doi.org/10.1007/BF02472447.

[5] K. Li, C. Li, Z. Chen, Influential depth of moisture transport in concrete subject to drying–wetting cycles, Cem. Concr. Compos. 31 (2009) 693–698, https://doi.org/10.1016/j.cemconcomp.2009.08.006.

[6] P. Lura, O.M. Jensen, K. van Breugel, Autogenous shrinkage in high-performance cement paste: an evaluation of basic mechanisms, Cem. Concr. Res. 33 (2003) 223–232, https://doi.org/10.1016/S0008-8846(02)00890-6.

[7] M. Schneider, The cement industry on the way to a low-carbon future, Cem. Concr. Res. 124 (2019), 105792, https://doi.org/10.1016/j.cemconres.2019.105792.

[8] K.L. Scrivener, B. Lothenbach, N. De Belie, E. Gruyaert, J. Skibsted, R. Snellings, A. Vollpracht, TC 238-SCM: hydration and microstructure of concrete with SCMs, Mater. Struct. 48 (2015) 835–862.

[9] E. Berodier, K. Scrivener, Evolution of pore structure in blended systems, Cem. Concr. Res. 73 (2015) 25–35.

[10] Q. Zeng, D. Zhang, H. Sun, K. Li, Characterizing pore structure of cement blend pastes using water vapor sorption analysis, Mater. Charact. 95 (2014) 72–84, https://doi.org/10.1016/j.matchar.2014.06.007.

[11] A. Vollpracht, B. Lothenbach, R. Snellings, J. Haufe, The pore solution of blended cements: a review, Mater. Struct. 49 (2016) 3341–3367.

[12] G. Andersson, S.-O. Ekman, Uncertainty about drying of new concrete, byggvarlden. https://www.byggvarlden.se/osakerhet-kring-uttorkning-av-ny-betong/, 2017.

[13] T. Luping, J. Gulikers, On the mathematics of time-dependent apparent chloride diffusion coefficient in concrete, Cem. Concr. Res. 37 (2007) 589–595, https://doi.org/10.1016/j.cemconres.2007.01.006.

[14] M.D.A. Thomas, P.B. Bamforth, Modelling chloride diffusion in concrete effect of fly ash and slag, Cem. Concr. Res. 9 (1999).

[15] V. Elfmarkova, P. Spiesz, H.J.H. Brouwers, Determination of the chloride diffusion coefficient in blended cement mortars, Cem. Concr. Res. 78 (2015) 190–199, https://doi.org/10.1016/j.cemconres.2015.06.014.

[16] M. Shafikhani, S.E. Chidiac, A holistic model for cement paste and concrete chloride diffusion coefficient, Cem. Concr. Res. 133 (2020), 106049, https://doi.org/10.1016/j.cemconres.2020.106049.

[17] N. Olsson, F. Abdul Wahid, L.-O. Nilsson, C. Thiel, H.S. Wong, V. Baroghel-Bouny, Wick action in mature mortars with binary cements containing slag or silica fume – the relation between chloride and moisture transport properties under non-saturated conditions, Cem. Concr. Res. 111 (2018) 94–103, https://doi.org/10.1016/j.cemconres.2018.06.006.

[18] V. Baroghel-Bouny, M. Thiéry, X. Wang, Modelling of isothermal coupled moisture–ion transport in cementitious materials, Cem. Concr. Res. 41 (2011) 828–841, https://doi.org/10.1016/j.cemconres.2011.04.001.

[19] M. Saeidpour, L. Wadsö, Moisture diffusion coefficients of mortars in absorption and desorption, Cem. Concr. Res. 83 (2016) 179–187, https://doi.org/10.1016/j.cemconres.2016.02.003.

[20] N. Olsson, L.-O. Nilsson, M. Åhs, V. Baroghel-Bouny, Moisture transport and sorption in cement based materials containing slag or silica fume, Cem. Concr. Res. 106 (2018) 23–32, https://doi.org/10.1016/j.cemconres.2018.01.018.

[21] O. Linderoth, P. Johansson, L. Wadsö, Development of pore structure, moisture sorption and transport properties in fly ash blended cement-based materials, Constr. Build. Mater. 261 (2020), 120007, https://doi.org/10.1016/j.conbuildmat.2020.120007.

[22] Q. Zeng, K. Li, T. Fen-chong, P. Dangla, Pore structure characterization of cement pastes blended with high-volume fly-ash, Cem. Concr. Res. 42 (2012) 194–204, https://doi.org/10.1016/j.cemconres.2011.09.012.

[23] Q. Huang, Z. Jiang, X. Gu, W. Zhang, B. Guo, Numerical simulation of moisture transport in concrete based on a pore size distribution model, Cem. Concr. Res. 67 (2015) 31–43, https://doi.org/10.1016/j.cemconres.2014.08.003.

[24] H. Ranaivomanana, J. Verdier, A. Sellier, X. Bourbon, Prediction of relative permeabilities and water vapor diffusion reduction factor for cement-based materials, Cem. Concr. Res. 48 (2013) 53–63, https://doi.org/10.1016/j.cemconres.2013.02.008.

[25] E.J. Garboczi, Permeability, diffusivity, and microstructural parameters: a critical review, Cem. Concr. Res. 20 (1990) 591–601, https://doi.org/10.1016/0008-8846(90)90101-3.

[26] P.J. Tumidajski, A.S. Schumacher, S. Perron, P. Gu, J.J. Beaudoin, On the relationship between porosity and electrical resistivity in cementitious systems, Cem. Concr. Res. 26 (1996) 539–544, https://doi.org/10.1016/0008-8846(96)00017-8.

[27] W. Wilson, F. Georget, K. Scrivener, Unravelling chloride transport/microstructure relationships for blended-cement pastes with the mini-migration method, Cem. Concr. Res. 140 (2021), 106264, https://doi.org/10.1016/j.cemconres.2020.106264.

[28] E. Astm, Standard Test Methods for Water Vapor Transmission of Materials, ASTM E96/E96M-13 Int. West Conshohocken PA. (96).

[29] L.-O. Nilsson, A comparison between different methods to determine moisture transport properties of cementitious materials, in: Report TVBM 3168 Building Materials, LTH, Lund University, 2013.

[30] L.-O. Nilsson, Moistenginst AB rapport 1922 (2019-10-03) (in Swedish). http://moistenginst.se/files/Burkmetoden_RAPPORT_1922_Moisture_Engineering_Institute_2019-10-03.pdf.

[31] L.-O. Nilsson, K. Bergström, The tin can method for determining moisture transport properties of concrete, in: E3S Web Conf, EDP Sciences, 2020, p. 14005.

[32] M. Saeidpour, L. Wadsö, Evidence for anomalous water vapor sorption kinetics in cement based materials, Cem. Concr. Res. 70 (2015) 60–66.

[33] T. Luping, L.-O. Nilsson, Rapid determination of the chloride diffusivity in concrete by applying an electric field, Mater. J. 89 (1993) 49–53.

[34] L. Greenspan, Humidity fixed points of binary saturated aqueous solutions, J. Res. Natl. Bur. Stand. Sect. Phys. Chem. 81A (1977) 89, https://doi.org/10.6028/jres.081A.011.

[35] L. Huang, L. Tang, I. Löfgren, N. Olsson, Z. Yang, Real-time monitoring the electrical properties of pastes to map the hydration induced microstructure change in cement-based materials, Cem. Concr. Compos. 132 (2022), 104639, https://doi.org/10.1016/j.cemconcomp.2022.104639.

[36] Z. Zhang, G.W. Scherer, Physical and chemical effects of isopropanol exchange in cement-based materials, Cem. Concr. Res. 145 (2021), 106461, https://doi.org/10.1016/j.cemconres.2021.106461.

[37] J. Crank, The Mathematics of Diffusion, Oxford University Press, 1979.

[38] G. Hedenblad, Moisture Permeability of Mature Concrete, Cement Mortar and Cement Paste, Lund University, 1993. PhD thesis.

[39] B. Perrin, V.B. Bouny, L. Chemloul, Methods of determination of the hydric diffusivity of hardened cement pastes, Mater. Struct. 31 (1998) 235–241.

[40] V. Zanjani Zadeh, C.P. Bobko, Nanoscale mechanical properties of concrete containing blast furnace slag and fly ash before and after thermal damage, Cem. Concr. Compos. 37 (2013) 215–221, https://doi.org/10.1016/j.cemconcomp.2012.09.003.

[41] M. Saeidpour, L. Wadsö, Moisture equilibrium of cement based materials containing slag or silica fume and exposed to repeated sorption cycles, Cem. Concr. Res. 69 (2015) 88–95, https://doi.org/10.1016/j.cemconres.2014.12.005.

[42] J. Skibsted, R. Snellings, Reactivity of supplementary cementitious materials (SCMs) in cement blends, Cem. Concr. Res. 124 (2019), 105799, https://doi.org/10.1016/j.cemconres.2019.105799.

[43] Z.P. Bažant, L.J. Najjar, Nonlinear water diffusion in nonsaturated concrete, Matér. Constr. 5 (1972) 3–20, https://doi.org/10.1007/BF02479073.

[44] K. Sakata, A study on moisture diffusion in drying and drying shrinkage of concrete, Cem. Concr. Res. 13 (1983) 216–224, https://doi.org/10.1016/0008-8846(83)90104-7.

[45] Apparent diffusivity model for concrete containing supplementary cementitious materials, ACI Mater. J. 110 (2013), https://doi.org/10.14359/51686338.

[46] K. Stanish, M. Thomas, The use of bulk diffusion tests to establish time-dependent concrete chloride diffusion coefficients, Cem. Concr. Res. 33 (2003) 55–62, https://doi.org/10.1016/S0008-8846(02)00925-0.

[47] M.D.A. Thomas, P.B. Bamforth, Modelling chloride diffusion in concrete effect of fly ash and slag, Cem. Concr. Res. 9 (1999).

[48] S. Diamond, Mercury porosimetry an inappropriate method for the measurement of pore size distributions in cement-based materials, Cem. Concr. Res. 9 (2000).

[49] J. Zhou, G. Ye, K. Van Breugel, Characterization of pore structure in cement-based materials using pressurization–depressurization cycling mercury intrusion porosimetry (PDC-MIP), Cem. Concr. Res. 40 (2010) 1120–1128.

[50] P. Mehta, P. Monteiro, Concrete: Microstructure, Properties, and Materials, McGraw-Hill Education, 2014.

[51] F. Avet, K. Scrivener, Investigation of the calcined kaolinite content on the hydration of limestone calcined clay cement (LC3), Cem. Concr. Res. 107 (2018) 124–135, https://doi.org/10.1016/j.cemconres.2018.02.016.

[52] B. Li, Q. Li, W. Chen, Spatial zonation of a hydrotalcite-like phase in the inner product of slag: new insights into the hydration mechanism, Cem. Concr. Res. 145 (2021), 106460, https://doi.org/10.1016/j.cemconres.2021.106460.

[53] S. Adu-Amankwah, M. Zajac, C. Stabler, B. Lothenbach, L. Black, Influence of limestone on the hydration of ternary slag cements, Cem. Concr. Res. 100 (2017) 96–109, https://doi.org/10.1016/j.cemconres.2017.05.013.

[54] F. Rajabipour, J. Weiss, Electrical conductivity of drying cement paste, Mater. Struct. 40 (2007) 1143–1160, https://doi.org/10.1617/s11527-006-9211-z.

[55] L. Huang, L. Tang, H. Gu, Z. Li, Z. Yang, New insights into the reaction of tricalcium silicate (C3S) with solutions to the end of the induction period, Cem. Concr. Res. 152 (2022), 106688, https://doi.org/10.1016/j.cemconres.2021.106688.

[56] D.L. Johnson, P.N. Sen, Dependence of the conductivity of a porous medium on electrolyte conductivity, Phys. Rev. B 37 (1988) 3502–3510, https://doi.org/10.1103/PhysRevB.37.3502.

[57] A. Revil, P.W.J. Glover, Theory of ionic-surface electrical conduction in porous media, Phys. Rev. B 55 (1997) 1757–1773, https://doi.org/10.1103/PhysRevB.55.1757.

[58] S.E. Chidiac, M. Shafikhani, Electrical resistivity model for quantifying concrete chloride diffusion coefficient, Cem. Concr. Compos. 113 (2020), 103707, https://doi.org/10.1016/j.cemconcomp.2020.103707.

[59] F.W. Locher, Cement: Principles of Production and Use, Verlag Bau+ Technik, 2013.

[60] I. García-Lodeiro, A. Fernández-Jiménez, A. Palomo, Variation in hybrid cements over time. Alkaline activation of fly ash–portland cement blends, Cem. Concr. Res. 52 (2013) 112–122, https://doi.org/10.1016/j.cemconres.2013.03.022.

[61] K.H. Coats, B.D. Smith, Dead-end pore volume and dispersion in porous media, Soc. Pet. Eng. J. 4 (1964) 73–84, https://doi.org/10.2118/647-PA.

[62] K. Schoone, J. Smets, R. Ramaekers, L. Houben, L. Adamowicz, G. Maes, Correlations between experimental matrix-isolation FT-IR and DFT(B3LYP) calculated data for isolated 1:1 H-bonded complexes of water and pyridine or imidazole derivatives, J. Mol. Struct. 649 (2003) 61–68, https://doi.org/10.1016/S0022-2860(03)00028-0.

[63] D. Hou, T. Li, P. Wang, Molecular dynamics study on the structure and dynamics of NaCl solution transport in the nanometer channel of CASH gel, ACS Sustain. Chem. Eng. 6 (2018) 9498–9509, https://doi.org/10.1021/acssuschemeng.8b02126.

[64] Q. Gui, M. Qin, K. Li, Gas permeability and electrical conductivity of structural concretes: impact of pore structure and pore saturation, Cem. Concr. Res. 89 (2016) 109–119, https://doi.org/10.1016/j.cemconres.2016.08.009.

[65] G.E. Archie, The electrical resistivity log as an aid in determining some reservoir characteristics, Trans. AIME 146 (1942) 54–62.

[66] E.R. Atkins, G.H. Smith, The significance of particle shape in formation resistivity factor-porosity relationships, J. Pet. Technol. 13 (1961) 285–291.

[67] E.J. Garboczi, Permeability, diffusivity, and microstructural parameters: a critical review, Cem. Concr. Res. 20 (1990) 591–601, https://doi.org/10.1016/0008-8846(90)90101-3.

[68] I.G. Richardson, S. Li, Composition and structure of an 18-year-old 5M KOH-activated ground granulated blast-furnace slag paste, Constr. Build. Mater. 168 (2018) 404–411, https://doi.org/10.1016/j.conbuildmat.2018.02.034.

[69] S.C. Taylor W.D. Hoff M.A. Wilson K.M. Green, Anomalous Water Transport Properties of Portland and Blended Cement-based Materials, (n.d.) 3.

[70] C. Zhou, F. Ren, Z. Wang, W. Chen, W. Wang, Why permeability to water is anomalously lower than that to many other fluids for cement-based material? Cem. Concr. Res. 100 (2017) 373–384, https://doi.org/10.1016/j.cemconres.2017.08.002.

[71] M.K. Moradllo, C. Qiao, B. Isgor, S. Reese, W.J. Weiss, Relating formation factor of concrete to water absorption, ACI Mater. J. 115 (2018) 887–898.